Journal of Science and Technology in Civil Engineering, HUCE, 2023, 17 (3): 140–153

UPPER BOUND LIMIT ANALYSIS OF SLOPE IN COHESIVE-FRICTIONAL SOILS USING THE NODE-BASED SMOOTHED FINITE ELEMENT METHOD

Thien Vo-Minh[a,*]

[a]*Faculty of Civil Engineering, HUTECH University,*
475A Dien Bien Phu street, Binh Thanh district, Ho Chi Minh City, Vietnam

Article history:
Received 06/02/2023, Revised 22/5/2023, Accepted 05/6/2023

Abstract

This paper presents the upper bound limit analysis of a slope in cohesive-frictional soils using the node-based smoothed finite element method (NS-FEM). The soil slope was discretized as triangular elements and modeled as Mohr-Coulomb material with the associated flow rule. This paper investigated the variation of slope stability numbers N_s with the change of the slope inclination angle α and β, and internal friction angle ϕ. Several numerical examples of slopes are presented, showing that the NS-FEM approach can demonstrate accuracy and efficiency solutions. Finally, the stability results are presented in design tables and charts for engineers to use in the preliminary design stage of the slope stability analysis.

Keywords: limit analysis; NS-FEM; slope stability; SOCP; upper bound.

https://doi.org/10.31814/stce.huce2023-17(3)-11

1. Introduction

Slope stability analysis has received wide attention because of its practical importance. Over several decades ago, the limit equilibrium method (LEM) has almost dominated in examining the stability of slopes, embankments, etc. Many researchers used the LEM for slope stability, including the works of Janbu [1], Morgenstern and Price [2], Spencer [3], Sarma [4], Fredlund and Krahn [5], Chen and Morgenstern [6] and others studies to satisfy the complete requirements for force and moment equilibrium. The method proposed by these researchers is useful because it can provide observation and insight into the studied problem. Although the accuracy of limit equilibrium solutions is based on the assumed failure mechanisms of slopes, this approach is often favored in the preliminary design stage because of its simplicity.

Another approach for analyzing geotechnical structure stability is using the lower and upper bound limit theorems developed by Drucker et al. [7]. Chen [8] applied the upper bound limit analysis to study slope stability problems using rigid-block failure mechanisms. Michalowski [9] performed a slope stability analysis based on a translation failure mechanism, which was assumed to be a rigid block analogous to slice in the traditional slice method. Donald and Chen [10] proposed a new method for stability analysis of slope in soils and rocks, where the sliding mass was divided into small numbers of discrete blocks with linear interfaces between blocks. Kim et al. [11] analyzed slopes using the limit equilibrium method and limit analysis and found that the results from the two approaches were in good agreement for homogeneous slopes. In recent years, Liu and Zhao [12], and Zhi-Bin and Chang-Bing [13] used the upper bound limit analysis based on the rigid finite element method in combination with linear or nonlinear programming for slope stability analysis. Recently, Seyed-Kolbadi et al. [14]

*Corresponding author. *E-mail address:* vm.thien@hutech.edu.vn (Vo-Minh, T.)

proposed an improved strength reduction based slope stability analysis. More recently, Vu-Hoang et al. [15] and Vo-Minh [16] used the bubble-enhanced quadrilateral element (FEM-Qi6) to evaluate the elastoplastic analysis of slope stability and the bearing capacity factors of strip footing in cohesive-frictional soils.

Some decades ago, the finite element method (FEM) was rapidly developing to solve complicated geotechnical problems. Sloan [17, 18], Sloan and Kleeman [19], Lyamin and Sloan [20, 21], and Krabbenhoft et al. [22] introduced finite element limit analysis (FELA) in combination using linear and non-linear optimization techniques for the stability of geotechnical problems. However, one of the drawbacks of low-order elements FEM-T3 is the volumetric locking phenomenon, which often occurs in nearly incompressible materials. To overcome disadvantages, many methods were suggested to reduce integration methods [23], enhance assumed strain [24–26], and so on. Another technique whose strain smoothing domains and the integration is performed over the cells associated with the nodes is the so-called node-based smoothed finite element method (NS-FEM). The node-based smoothed finite element method has been employed for upper bound limit problems due to the following advantages: (i) total degrees of freedom significantly decreased, leading to a fast convergence for solutions, (ii) volumetric locking phenomenon is prevented by using the NS-FEM method in solving undrained geotechnical analysis, (iii) by using of smoothed strains in NS-FEM, the integration is conducted in the edges of smoothed cells, there is no need to calculate the derivatives of the shape function. Liu et al. [27] and Nguyen-Xuan et al. [28] applied this method to calculate the limit and shakedown loads in solid mechanics problems made of elastic-perfectly plastic material. The NS-FEM recently became an active research topic that has been widely applied to heat transfer analysis (Wu et al. [29]), fracture analysis (Liu et al. [30]), structural-acoustic analysis of shells (Wang et al. [31]). Recently, Vo-Minh et al. [32–34] applied NS-FEM for the stability of circular tunnels, dual circular, and dual square tunnels in cohesive-frictional soils. More recently, Vo-Minh [35] estimated strip footing bearing capacity factors using the node-based smoothed finite element method and second-order cone programming using the upper limit analysis.

This paper presents the application of the NS-FEM for stability analysis of natural slopes in homogeneous cohesive-frictional soils using the upper bound limit analysis and second-order cone programming (SOCP) optimization. To consider the slope stability analysis, a dimensionless stability factor N_s can be presented by three parameters: slope inclination angle α and β, soil friction angle ϕ. Several numerical results of slopes have been investigated, showing that the NS-FEM approach can demonstrate accuracy and efficiency solutions. The stability results are presented in design tables and charts for engineers to use in the preliminary design stage of the slope stability analysis.

The article is organized as follows: Section 2 describes the problem definition. Section 3 presents an upper bound limit analysis for a plane strain with the Mohr-Coulomb yield criterion. Numerical examples are presented in Section 4. Finally, Section 5 closes this paper with some concluding remarks.

2. Problem definition

Fig. 1 shows a general layout of the slope stability analysis with a height H and the slope inclination angle α and β. Under plane strain conditions, the homogeneous soil properties are the cohesion c, friction angle ϕ and unit weight γ. According to the upper bound limit analysis theorem, the soil behaves as a perfectly plastic material and obeys the associated flow rule following the Mohr-Coulomb failure criterion.

A typical finite element mesh for the stability analysis of the slope problem is illustrated in Fig. 2. The boundary conditions of this problem were such that the model's left, right and bottom boundaries

were fixed in both the horizontal and vertical directions. Therefore, the size of the problem domain is chosen to be large enough to eliminate the boundary effects and the plastic zones to be contained entirely within the domain and not intersect the right and bottom boundaries.

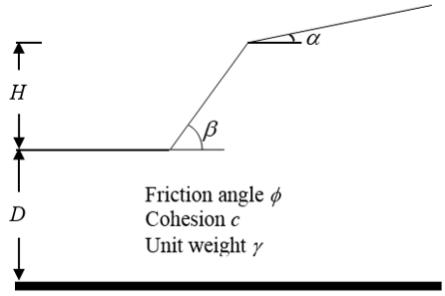

Figure 1. Soil properties and geometry of the slope

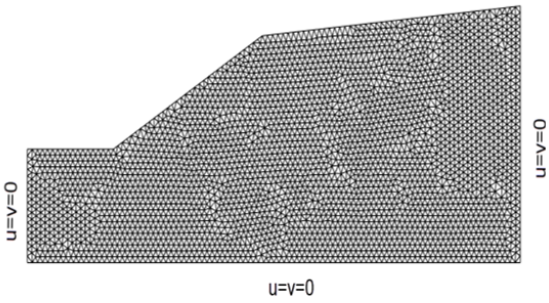

Figure 2. Typical finite element mesh and displacement boundary conditions for the case $\alpha = 5^\circ, \beta = 30^\circ$

To evaluate the stability of a slope under the influence of the soil cohesion and self-weight, a dimensionless stability factor N_s can be presented by three input parameters such as slope inclination angle α and β, soil friction angle ϕ

$$N_s = \frac{\gamma H}{c} = f(\alpha, \beta, \phi) \tag{1}$$

where $N_s = \gamma H/c$ is the stability factor proposed by Chen [8], then various researchers developed stability charts under plane-strain conditions, such as Lyamin and Sloan [20, 21], Krabbenhoft et al. [22], Makrodimopoulous and Martin [36].

This paper considers the slope angles $\alpha = 0^\circ$ - 25°, $\beta = 30^\circ$ - 90°, and the value of friction angles $\phi = 0^\circ$ - 35°. To obtain an upper bound solution for the stability factor N_s of slope, it is convenient to consider $c = 1$, $\gamma = 1$. In this case, the stability factor $N_s = H_c$ may be used to predict the critical height H_c of an embankment with slope angle α and β.

3. Upper bound limit analysis for slope stability using a node-based smoothed finite element method (NS-FEM)

3.1. A brief overview of the NS-FEM

Unlike the traditional finite element method (FEM), the numerical integration domains of the node-based smoothing method (NS-FEM) are based on polygonal cells related to the nodes rather than the elements. The problem domain Ω is divided into N_s smoothing cells formulated as $\Omega = \sum_{k=1}^{N_s} \Omega_k^s$ and $\Omega_i^s \cap \Omega_j^s = \varnothing$, $i \neq j$ and N_s is the total number of field nodes in the entire problem domain. The polygonal cells Ω_k^s called a nodal smoothing domain associated with the node k, are constructed by connecting the mid-edge points sequentially to the centroid of surrounding triangular elements, as shown in Fig. 3. The smoothing domain boundary Ω_k^s is labeled as Γ_k, and the union of all Ω_k^s forms precisely the whole problem Ω.

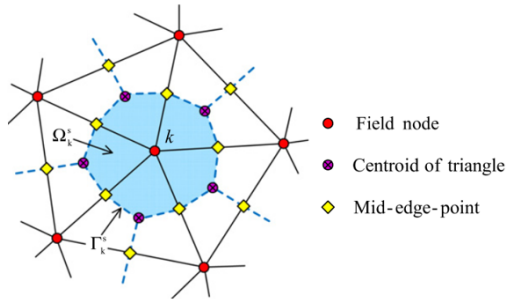

Figure 3. The smoothing cells associated with the nodes in the NS-FEM

The smoothed strain on the cell Ω_k^s associated with node k using NS-FEM can be calculated by

$$\tilde{\dot{\boldsymbol{\varepsilon}}}_k = \sum_{k \in N^{(s)}} \tilde{\mathbf{B}}_k(\mathbf{x}_s)\mathbf{d}_k \tag{2}$$

where $N^{(s)}$ is the set containing nodes directly connected to node k, $\mathbf{d}_k$ is the nodal displacement vector, and the smoothed strain gradient matrix $\tilde{\mathbf{B}}_k(\mathbf{x}_s)$ on the domain $\wedge_k^s$ can be determined from

$$\tilde{\mathbf{B}}_k(\mathbf{x}_s) = \begin{bmatrix} \tilde{b}_{kx}(x_s) & 0 \\ 0 & \tilde{b}_{ky}(x_s) \\ \tilde{b}_{ky}(x_s) & \tilde{b}_{kx}(x_s) \end{bmatrix} \tag{3}$$

where

$$\tilde{b}_{kh}(x_s) = \frac{1}{A_k^{(s)}} \int_{\Gamma_k} \mathbf{n}_h^{(s)}(\mathbf{x}) N_k(\mathbf{x}) \mathrm{d}\Gamma \tag{4}$$

where $A_k^{(s)} = \int_{\Omega_k^s} d\Omega$ is the area of the cell Ω_k^s, $N_k(\mathbf{x})$ is the FEM shape function for node k, and $\mathbf{n}^{(s)}(\mathbf{x})$ is the normal outward vector on the boundary $\Gamma_k^{(s)}$. The number of Gauss points for line integration (4) depends on the degree of N_k. If N_k are linear shape functions, one Gauss point is sufficient for line integration along each segment of a boundary of $\Gamma_k^{(s)}$ of Ω_k^s, Eq. (4) can be transformed to its algebraic form

$$\tilde{b}_{kh}(x_s) = \frac{1}{A_k^{(s)}} \sum_{k=1}^{M} \mathbf{N}_k(\mathbf{x}_k^{GP}) n_{kh}^{(s)} l_k^{(s)}, \quad (h = x, y) \tag{5}$$

where M is the total of the boundary segment of $\wp_k^{(s)}$, $\mathbf{x}_i^{GP}$ is the Gauss point of the boundary segment of $\wp_k^{(s)}$, which has length $l_k^{(s)}$ and outward unit normal $n_{kh}^{(s)}$.

3.2. An upper bound limit analysis for a plane strain in geotechnical problems using the NS-FEM

A two-dimensional problem domain $\wedge$ bounded by a continuous boundary $S_{\dot{\mathbf{u}}} \cup S_{\mathbf{t}} = S, S_{\dot{\mathbf{u}}} \cap S_{\mathbf{t}} = \varnothing$ is considered. The rigid-perfectly plastic body is subjected to external tractions $\mathbf{g}$ on $S_{\mathbf{t}}$ and body forces $\mathbf{f}$ on the boundary $S_{\dot{\mathbf{u}}}$ prescribed by the displacement velocity vector $\dot{\mathbf{u}}$. The strain rates can be expressed by equation

$$\dot{\varepsilon} = \begin{bmatrix} \dot{\varepsilon}_{xx} & \dot{\varepsilon}_{yy} & \dot{\gamma}_{xy} \end{bmatrix}^T = \nabla \dot{\mathbf{u}} \tag{6}$$

In the upper bound theorem, a kinematically admissible displacement field $\dot{\mathbf{u}} \in U$, such that

$$W_{int}(\boldsymbol{\sigma}, \dot{\mathrm{u}}) = \alpha^+ W_{\mathrm{ext}}(\dot{\mathbf{u}}) \tag{7}$$

where α^+ is the limit load multiplier of the external tractions load $\mathbf{g}$ and body forces $\mathbf{f}$.

The external work can be determined

$$W_{ext}(\dot{\mathbf{u}}) = \int_{\Omega} \mathbf{f}\dot{\mathbf{u}} d\Omega + \int_{\Gamma_t} \mathbf{g}\dot{\mathbf{u}} dS \tag{8}$$

The internal plastic dissipation of the two-dimensional domain $\wedge$ can be written as

$$W_{int}(\boldsymbol{\sigma}, \dot{\mathbf{u}}) = \int_{\Omega} D_p(\dot{\mathbf{u}}) d\Omega = \int_{\Omega} \boldsymbol{\sigma}\dot{\boldsymbol{\varepsilon}} d\Omega \tag{9}$$

in which a space of kinematically admissible velocity field is denoted by

$$U = \left\{ \dot{\mathbf{u}} \in (H^1(\Omega))^2, \dot{\mathbf{u}} = \bar{\dot{\mathbf{u}}} \quad \text{on } S_{\dot{\mathbf{u}}} \right\} \tag{10}$$

Setting $C = \{\dot{\mathbf{u}} \in U | W_{ext}(\dot{\mathbf{u}}) = 1\}$, the limit analysis problem is based on the kinematical theorem to determine the collapse multiplier α^+ of the following optimization problem

$$\begin{aligned} &\alpha^+ = \max \{\exists \boldsymbol{\sigma} \in \sum | W_{int}(\boldsymbol{\sigma}, \dot{\mathbf{u}}) = \alpha W_{ext}(\dot{\mathbf{u}}), \forall \dot{\mathbf{u}} \in U\} = \min_{\dot{\mathbf{u}} \in U} D_p(\dot{\mathbf{u}}) \\ &st \begin{cases} \dot{\mathbf{u}} = 0 \quad \text{on } S_u \\ W_{ext}(\dot{\mathbf{u}}) = 1 \end{cases} \end{aligned} \tag{11}$$

In geotechnical problems, Makrodimopoulos and Martin [36] proposed the internal plastic dissipation equation for plane strain as follows

$$D_p(\dot{\mathbf{u}}) = c \cos\phi \int_\Omega \sqrt{(\tilde{\varepsilon}^i_{xx} - \tilde{\varepsilon}^i_{yy})^2 + (\tilde{\gamma}^i_{xy})^2} d\Omega \tag{12}$$

where c, ϕ are the cohesion and friction angle of the soil, respectively.

For an associated flow rule, the plastic strain rates vector is given by

$$\dot{\boldsymbol{\varepsilon}} = \lambda \frac{\partial \psi(\boldsymbol{\sigma})}{\partial \boldsymbol{\sigma}} \tag{13}$$

where λ is a non-negative the plastic multiplier and the Mohr-Coulomb yield function $\psi(\boldsymbol{\sigma})$ can be expressed in the form of stress components as

$$\psi(\boldsymbol{\sigma}) = \sqrt{(\sigma_{xx} - \sigma_{yy})^2 + 4\tau^2_{xy}} + (\sigma_{xx} + \sigma_{yy}) \sin\phi - 2c \cos\phi \tag{14}$$

Using the NS-FEM, the problem is discretized by N_e triangular elements and the total number of nodes N_n. The smoothed strains rates $\tilde{\boldsymbol{\varepsilon}}$ can be calculated from Eq. (1). The upper bound limit analysis for a plane strain of slope stability using the Mohr-Coulomb failure criterion can be written

$$\begin{aligned} &\alpha^+ = N_s = \min \left(\sum_{i=1}^{N_n} cA_i \cos\phi \sqrt{(\tilde{\varepsilon}^i_{xx} - \tilde{\varepsilon}^i_{yy})^2 + (\tilde{\gamma}^i_{xy})^2} - W^0_{ext}(\dot{\mathbf{u}}) \right) = \min \left(\sum_{i=1}^{N_n} cA_i t_i \cos\phi - W^0_{ext}(\dot{\mathbf{u}}) \right) \\ &st \begin{cases} \dot{\mathbf{u}} = 0 \quad \text{on } S_{\mathbf{u}} \\ W_{ext}(\dot{\mathbf{u}}) = 1 \\ \tilde{\varepsilon}^i_{xx} + \tilde{\varepsilon}_{yy} = t_i \sin\phi \\ t_i \geq \sqrt{(\tilde{\varepsilon}^i_{xx} - \tilde{\varepsilon}^i_{yy})^2 + (\tilde{\gamma}^i_{xy})^2}, \; i = 1, 2, \ldots, N_n \end{cases} \end{aligned} \tag{15}$$

where α^+ is a stability number, A_i is the area of node i, and N_n is the total number of nodes in the domain. The last constraint in Eq. (15) is expressed in the conic form. As a result, the conic interior-point optimizer of the academic Mosek package [37] is used to solve this problem. The upper bound using the NS-FEM approach has been written in Matlab. The computations were performed on a Windows XP environment in a Dell Optiplex 990 (Intel CoreTM i5, 1.6GHz CPU, 8GB RAM).

4. Numerical examples

4.1. Comparisons of slope failure mechanisms and stability factors with other solutions

In order to obtain the stability factor N_s representing the effect of the soil weight and cohesion ($\gamma = 1$, $c = 1$), the optimization problem for plane strain using the NS-FEM can be determined by $\alpha^+ = N_s = \min\left(\sum_{i=1}^{N_n} A_i t_i \cos\phi - W^0_{ext}(\dot{\mathbf{u}})\right)$.

For comparison purposes, the power dissipations of slopes using the NS-FEM and Krabbenhoft et al. [22] solution for the case $\beta = 60^\circ$, $\alpha = 0^\circ$, $\phi = 20^\circ$ is shown in Fig. 4. The surface of sliding using the NS-FEM is passing through the toe of the slope, illustrated in Fig. 4(a). It is clear that the failure mechanism obtained using the NS-FEM is quite the same as that of the solution reported by Krabbenhoft et al. [22] in Fig. 4(b).

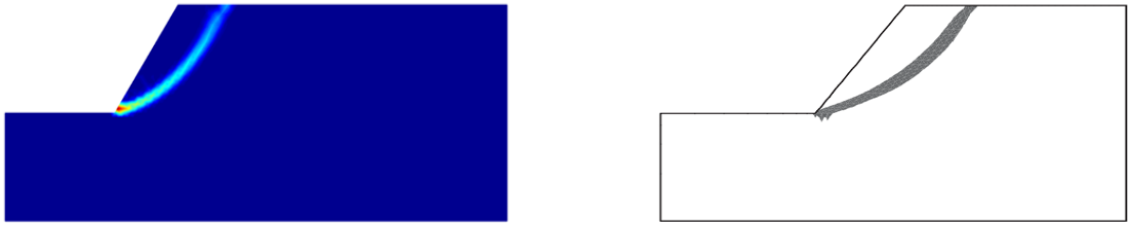

(a) Power dissipation using the NS-FEM

(b) Power dissipation reported by Krabbenhoft et al. [22]

Figure 4. Comparison of the power dissipation between NS-FEM and solution reported by Krabbenhoft et al. [22] for $\beta = 60^\circ$, $\alpha = 0^\circ$, $\phi = 20^\circ$, $c = 1$

The results of stability numbers N_s of slopes obtained from the present study were compared with other numerical results in the cases β from 50° to 90°: (1) Chen [8] used the upper bound rigid-block failure mechanisms; (2) Lyamin and Sloan [20, 21] used the upper bound and lower bound solutions and non-linear programming optimization; (3) Krabbenhoft et al. [22] used 3-node elements with discontinuities and non-linear optimization. A comparison of these results is listed in Table 1 for the cases $\beta = 50^\circ$ - 90°. The $N_s$values are in good agreement with the analytical upper bound solution of Chen [8] and the average values of the lower bound and the upper bound theorem reported by Lyamin and Sloan [20, 21]. The results of N_s using the NS-FEM are smaller than those of Krabbenhoft et al. [22], with a maximum error of 2.2%. A comparison of stability numbers N_s used the present method to show the accuracy and convergence of the NS-FEM for solving the slope stability analysis.

Table 1. Comparison of the stability number of slope N_s between NS-FEM and other solutions in the literature ($\phi = 20^\circ$)

β	Chen [8]	Lyamin & Sloan [21]	Lyamin & Sloan [20]	Krabbenhoft et al. [21]	NS-FEM
	UB	UB	LB	UB	UB
50	13.63	13.79	13.44	13.79	13.55
60	10.39	10.54	10.21	10.54	10.30
70	8.30	8.44	8.12	8.44	8.27
80	6.75	6.89	6.58	6.89	6.68
90	5.50	5.67	5.41	5.67	5.45

UB - Upper bound; LB - Lower bound

To consider the accuracy of this approach, a comparison of the stability numbers N_s, the number of iterations, and optimization CPU times using the NS-FEM with those reported by Makrodimopoulous and Martin [36] are listed in Table 2. The reported CPU times refer to the time spent on the interior-point iterations and exclude the time to read the data file. For slope stability, Makrodimopoulous and Martin [36] used 28864 3-node elements with discontinuities (FEM-T3) and 6-node triangular elements (FEM-T6) in the mesh.

It is evident that the slope stability factor based on the NS-FEM for the case $\beta = 70^\circ$, $\phi = 35^\circ$ solutions ($N_s = 13.95$) using 6834 triangular elements agree well with the 6-node triangular element presented by Makrodimopoulous & Martin [36] using a mesh of 28864 triangular elements ($N_s = 13.88$), with the error is less than 0.64%. Furthermore, based on an interior-point algorithm using the Mosek optimizer, the NS-FEM optimization problem is very fast convergence, with about 22 - 24 step iterations and a maximum CPU time of 3.11 s. Thus, the numerical procedure using the NS-FEM and SOCP reduces a significant number of elements and the time for solving optimization problems.

Table 2. Comparison of the stability number of slope N_s for the case $\beta = 70^\circ$

Makrodimopoulos and Martin [36]					NS - FEM	
($\phi = 20^\circ$)		($\phi = 35^\circ$)			($\phi = 20^\circ$)	($\phi = 35^\circ$)
	FEM - T3	FEM - T6	FEM - T3	FEM - T6	NS - FEM	NS - FEM
N_e	N_s (Error %) Iterations CPU (s)	N_s (Error %) Iterations CPU (s)	N_s (Error %) Iterations CPU (s)	N_s (Error %) Iterations CPU (s)	N_e	N_s (Error %) Iterations CPU (s)	N_s (Error %) Iterations CPU (s)
28864	8.471 (2.06%) 23 65.1 (s)	8.338 (0.46%) 36 194.5 (s)	15.46 (11.57%) 29 85.2 (s)	14.19 (2.41%) 21 109.5 (s)	6834	8.275 (- 0.3%) 22 3.3 (s)	13.95 (0.64%) 24 3.11 (s)

N_e - no. of elements

4.2. Numerical results and discussions

In this study, the weight of the soil considered as the external force contributes to the stability factors N_s. Generally, there are two distinct failure modes for the slope stability analysis:

(a) Toe failure mode: the sliding surface passes through the toe of the slope for all cases $\beta \leq 60^\circ$ and $\phi \geq 10^\circ$ because the friction angle ϕ increases, leading to the frictional component of shear strength of the soil slope increasing.

(b) Base failure mode: the failure mechanisms extend beneath the toe of the slope in the case $\beta \leq 60^\circ$, $\alpha = 0^\circ$ to 15°, and slight friction angle $\phi = 0^\circ$ to 5°. In this failure mode, the energy dissipation by the soil shear strength is slightly greater than or equal to the self-weight of the soil.

Fig. 5 shows the plastic dissipation distribution of the slope using the present method NS-FEM in the case $\beta = 30^\circ$, $\phi = 0^\circ$, $\alpha = 0^\circ$, and $\alpha = 15^\circ$. For a purely cohesive soil (friction angle $\phi = 0^\circ$) as shown in Figs. 5(a)–5(b), failure surfaces pass below the toe of the slope because of the sliding due to gravity, which tends to mobilize a larger volume of shear resistance than those of toe failure mode.

Figs. 6(a), 6(c), 7(a), 7(c) show the failure mechanisms of slopes for the cases $\beta = 30^\circ$- 60°, $\alpha = 0^\circ$ and 15°, small friction angle $\phi = 5^\circ$. In these figures, the sliding surfaces beneath the toe of the slope tend to mobilize a larger volume of shear resistance than those of toe failure mode because the

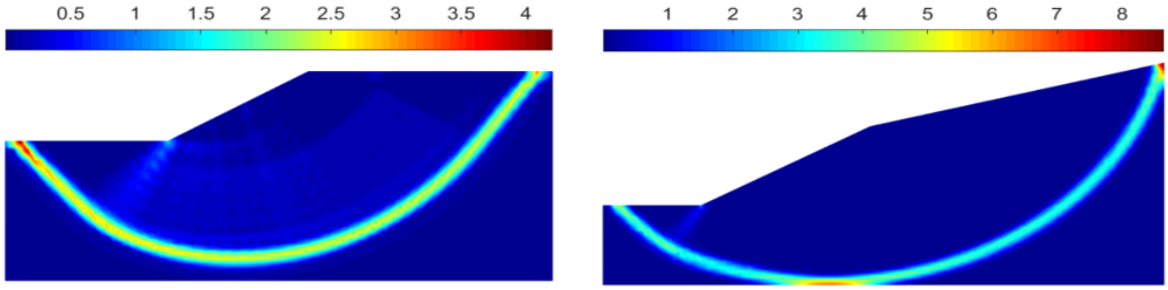

(a) $\alpha = 0^\circ$ (b) $\alpha = 15^\circ$

Figure 5. Power dissipation of the slope using NS-FEM for the case $\beta = 30^\circ$, $\phi = 0^\circ$

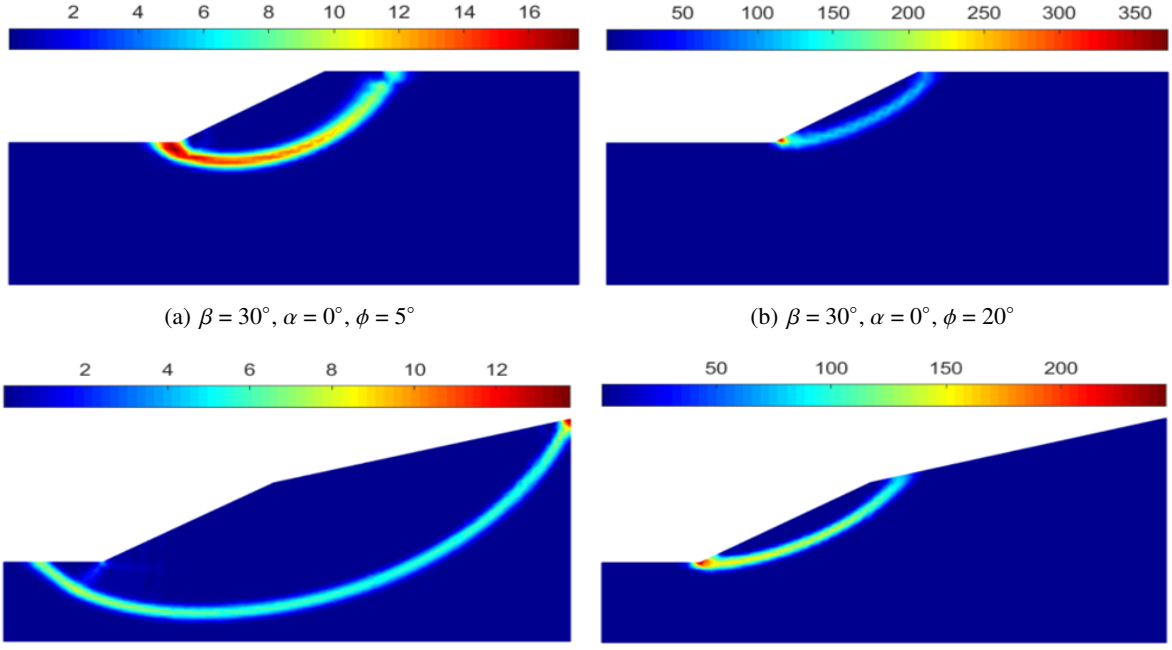

(a) $\beta = 30^\circ$, $\alpha = 0^\circ$, $\phi = 5^\circ$ (b) $\beta = 30^\circ$, $\alpha = 0^\circ$, $\phi = 20^\circ$

(c) $\beta = 30^\circ$, $\alpha = 15^\circ$, $\phi = 5^\circ$ (d) $\beta = 30^\circ$, $\alpha = 15^\circ$, $\phi = 20^\circ$

Figure 6. Power dissipations of slope using NS-FEM for the case β =30°

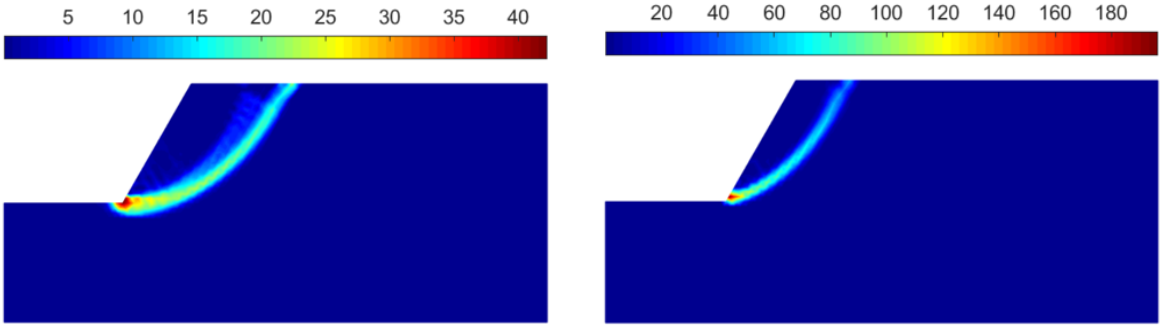

(a) $\beta = 60^\circ$, $\alpha = 0^\circ$, $\phi = 5^\circ$ (b) $\beta = 60^\circ$, $\alpha = 0^\circ$, $\phi = 20^\circ$

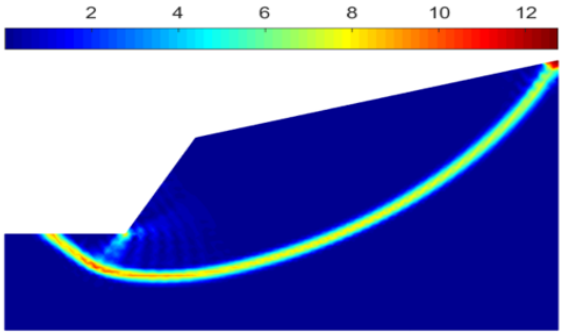

(c) $\beta = 60^\circ$, $\alpha = 15^\circ$, $\phi = 5^\circ$

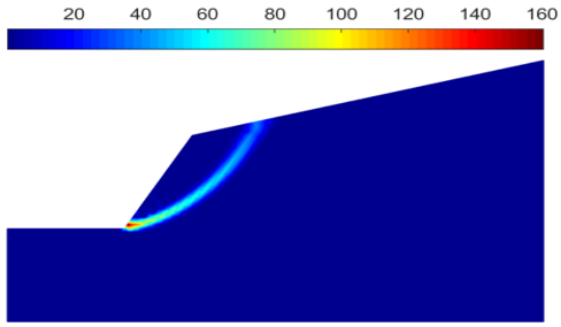

(d) $\beta = 60^\circ$, $\alpha = 15^\circ$, $\phi = 20^\circ$

Figure 7. Power dissipations of slope using NS-FEM for the case β =60°

shear strength of the soil slope is small. When the friction angle increases $\phi = 20^\circ$, the failure surfaces develop from the toe of the slope and extend to the ground surface, as illustrated in Figs. 6(b), 6(d), 7(b), 7(d). It means that the shear strength of the soil slope increases with an increase in friction angle ϕ, and the toe failure mechanism occurs.

Fig. 8 illustrates failure mechanisms of the slope in the cases $\beta = 90^\circ$, $\alpha = 0^\circ$ - 15°, $\phi = 5^\circ$ - 20°, the failure surfaces develop from the toe of the slope and extend to the ground surface.

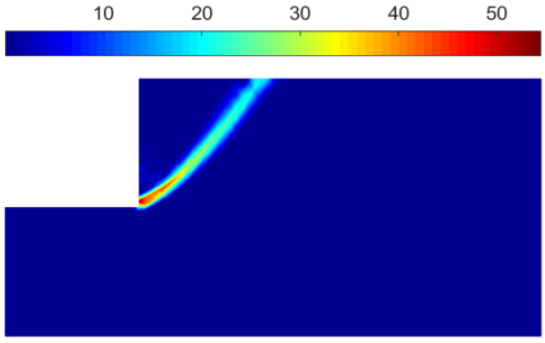

(a) $\beta = 90^\circ$, $\alpha = 0^\circ$, $\phi = 5^\circ$

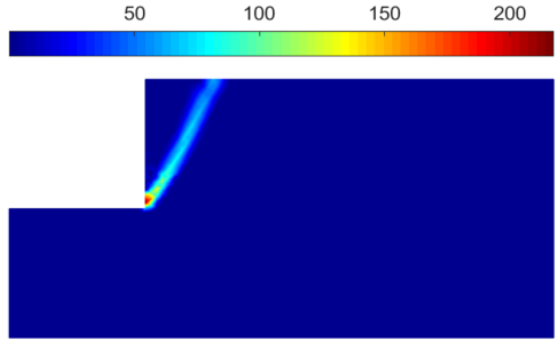

(b) $\beta = 90^\circ$, $\alpha = 0^\circ$, $\phi = 20^\circ$

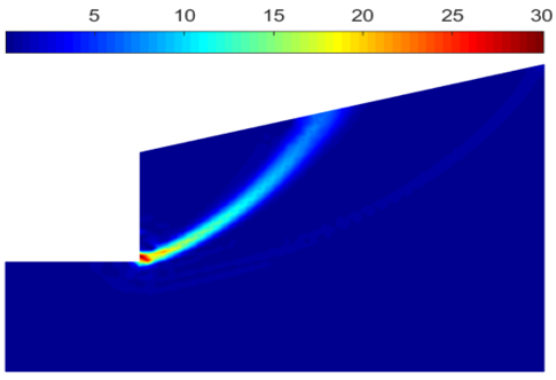

(c) $\beta = 90^\circ$, $\alpha = 15^\circ$, $\phi = 5^\circ$

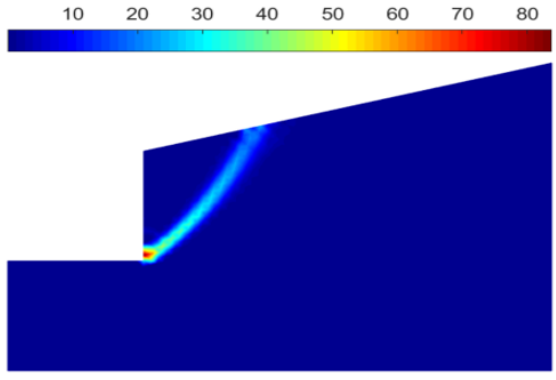

(d) $\beta = 90^\circ$, $\alpha = 15^\circ$, $\phi = 20^\circ$

Figure 8. Power dissipations of slope using NS-FEM for the case $\beta = 90^\circ$

Fig. 9 shows the transition zone of slope failure mechanisms and the relationship between stability factors N_s and small friction angles $\phi = 0^\circ$ - 10°, slope angles $\alpha = 0^\circ$ - 5° and $\beta = 30^\circ$ - 90°. Comparisons indicate that the effect of friction angle ϕ on the failure mechanism is significant compared to other parameters. As shown in Figs. 9-9(b), there are two distinct failure modes for the slope stability analysis: i) When $\beta \leq 60^\circ$, α ranging from 0° to 5°, and friction angle $\phi = 0^\circ$ to 5°, the base failure mechanisms beneath the toe of the slope because the shear strength of the soil slope is small; ii) In the cases $\beta \leq 60^\circ$, $\phi \geq 10^\circ$ and $\beta > 60^\circ$, $\phi > 0^\circ$, the sliding failure surface passes through the toe of the slope because an increase in the friction angle contributes to an increase the shear strength of the soil slope.

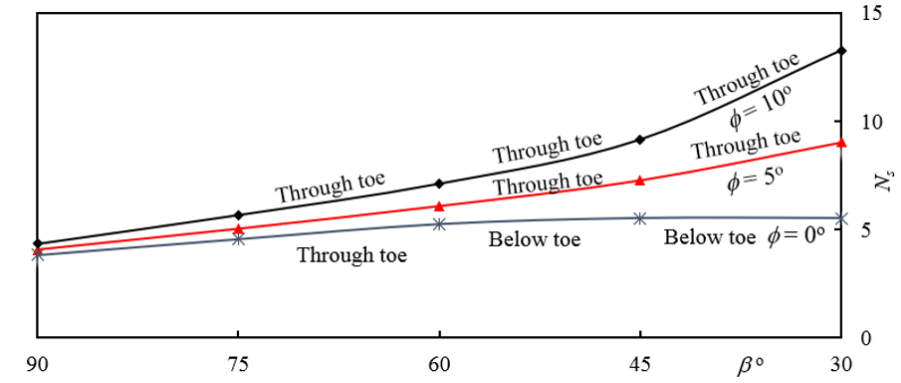

(a) $\alpha = 0^\circ$

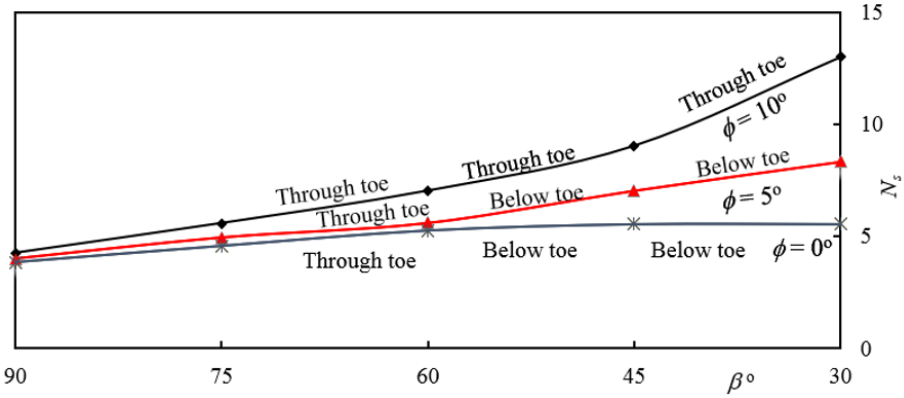

(b) $\alpha = 5^\circ$

Figure 9. Stability numbers of slope N_s using NS-FEM

The computed values of N_s for friction angles ϕ ranging from 5° to 35°, slope angles α from 0° to 25°, and β ranging from 30° to 90° using the NS-FEM are summarized in Table 3.

The variation of stability factors N_s with the effect of the inclination angle of slope β (for different friction angle values ϕ) is plotted in Fig. 10 for the case $\alpha = 0^\circ$. From Fig. 10, the N_s values decreased as the slope angle β increased. The rate of reduction in N_s rapidly when β ranges from 30° to 45° and the friction angle is slight $\phi = 5^\circ$. However, the magnitude of N_s decreased linearly when the friction angle $\phi = 35^\circ$. The stability factors obtained from the present method NS-FEM are well in agreement with the analytical upper bound solution reported by Chen [8]. It demonstrates that the present method has high effectiveness for solving slope stability analysis in cohesive-frictional soils.

Table 3. The stability numbers of slope N_s between NS-FEM and results reported by Chen [8]

ϕ°	α°	$\beta = 30^\circ$		$\beta = 45^\circ$		$\beta = 60^\circ$		$\beta = 75^\circ$		$\beta = 90^\circ$	
		NS-FEM	Chen [8]	NS-FEM	Chen [8]	NS-FEM	Chen [8]	NS-FEM	Chen [8]	NS-FEM	Chen [8]
5	0	9.03	9.13	7.27	7.35	6.08	6.16	5.03	5.14	4.06	4.19
	5	8.33	8.83	7.03	7.18	5.88	6.03	4.93	5.05	3.98	4.14
10	0	13.28	13.50	9.16	9.31	7.12	7.26	5.67	5.80	4.34	4.58
	5	12.98	13.28	9.02	9.16	7.02	7.14	5.57	5.71	4.24	4.53
	10	12.28	12.89	8.45	8.93	6.55	6.94	5.33	5.61	4.17	4.47
15	0	21.57	21.69	11.94	12.05	8.35	8.63	6.27	6.57	4.95	5.02
	5	20.98	21.48	11.44	11.91	8.24	8.52	6.17	6.49	4.85	4.97
	10	20.63	21.14	11.03	11.72	8.08	8.38	6.07	6.38	4.75	4.91
	15	20.24	20.49	10.87	11.42	7.98	8.19	5.98	6.26	4.63	4.83
20	0	41.07	41.22	16.06	16.16	10.33	10.39	7.24	7.48	5.45	5.50
	5	40.87	41.02	15.89	16.03	10.09	10.28	7.08	7.40	5.24	5.46
	10	40.45	40.69	15.44	15.84	9.85	10.16	6.99	7.30	5.17	5.40
	15	39.97	40.09	15.19	15.58	9.47	9.98	6.78	7.18	5.08	5.33
	20	38.24	38.64	14.97	15.17	9.26	9.74	6.54	7.03	5.01	5.24
25	0	118.19	119.93	22.76	22.90	12.25	12.74	8.34	8.58	5.95	6.06
	5	118.01	119.70	22.69	22.77	12.18	12.64	8.20	8.50	5.85	6.01
	10	117.89	119.35	22.51	22.60	12.07	12.52	8.11	8.41	5.78	5.95
	15	117.23	118.79	22.19	22.35	11.92	12.36	7.96	8.30	5.70	5.89
	20	116.98	117.43	21.75	21.98	11.65	12.14	7.67	8.16	5.60	5.80
	25	111.54	112.07	20.96	21.35	11.28	11.84	7.42	7.97	5.49	5.70
30	0	-	-	35.16	35.54	15.89	16.04	9.65	9.94	6.47	6.69
	5	-	-	35.06	35.41	15.69	15.94	9.45	9.86	6.37	6.64
	10	-	-	34.93	35.25	15.58	15.82	9.38	9.77	6.25	6.59
	15	-	-	34.67	35.01	15.44	15.67	9.30	9.67	6.08	6.52
	20	-	-	34.23	34.67	15.19	15.47	9.21	9.54	5.89	6.44
	25	-	-	33.96	34.11	15.02	15.20	9.15	9.37	5.73	6.35
35	0	-	-	65.24	65.52	20.53	20.94	11.37	11.68	7.25	7.42
	5	-	-	65.14	65.52	20.43	20.84	11.26	11.60	7.15	7.38
	10	-	-	64.95	65.22	20.27	20.73	11.20	11.51	7.09	7.32
	15	-	-	64.45	64.70	20.17	20.59	11.08	11.36	7.02	7.26
	20	-	-	64.39	64.65	20.09	20.40	11.01	11.29	6.92	7.19
	25	-	-	64.05	64.12	19.98	20.14	10.94	11.13	6.81	7.10

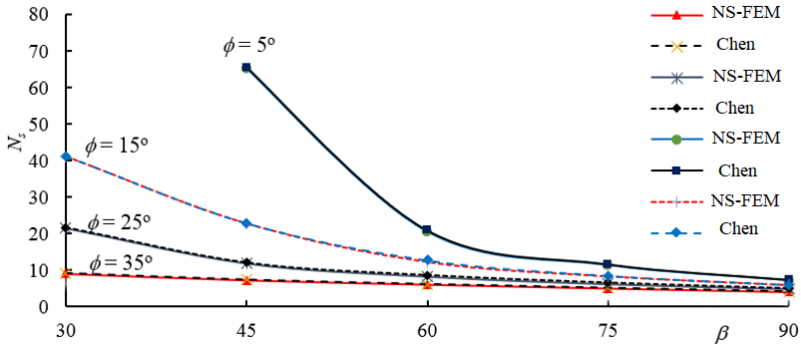

Figure 10. Comparison stability factors N_s of slopes using NS-FEM and Chen [8] solution in the case $\alpha = 0°$

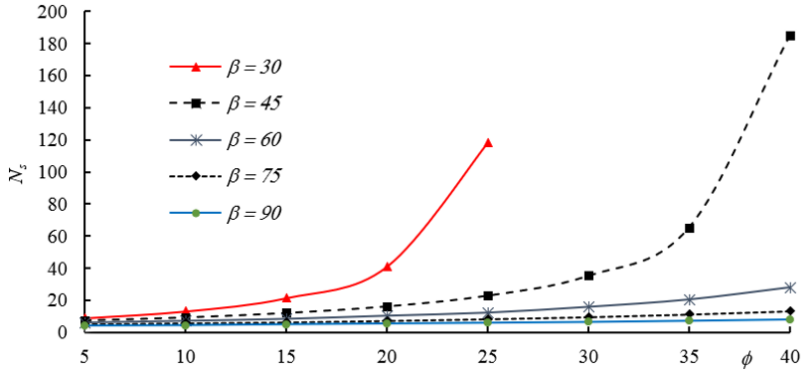

Figure 11. Stability factors N_s of slopes using NS-FEM in the case $\alpha = 0°$

Fig. 11 shows the relationship between the stability factors N_s of slopes at different inclination slope angles β =30° - 90° and friction angle $\phi = 5°$ - 35° for the case $\alpha = 0°$. In Fig. 11, it can be seen that the values of N_s increased with an increase of ϕ. It means that friction angle ϕ contributes to the increase in the frictional component of shear resistance of soil slope.

Fig. 12 illustrates the variation of stability factors N_s with the change of the friction angle ϕ for different values of $\beta$and $\alpha = 5°$, $\alpha = 15°$. From Fig. 12, the values of N_s increased with an increase of ϕ, and the results of N_s slightly decreased with an increase of the slope inclination angle α.

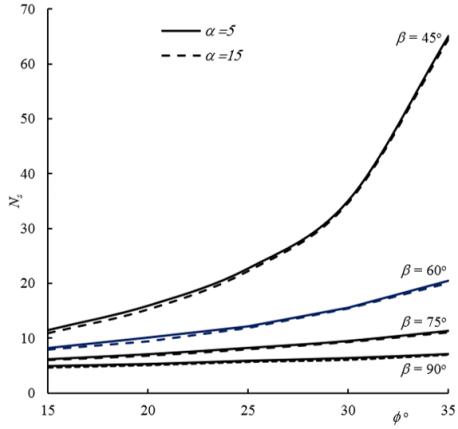

Figure 12. Stability factors N_s of slopes using NS-FEM in the case $\alpha = 5°$ and $\alpha = 15°$

5. Conclusions

This paper proposes a node-based smoothed finite element method (NS-FEM) to evaluate homogeneous slope stability in cohesive-frictional soils. Design tables and dimensionless charts are investigated with the various soil friction angles ϕ and slope inclination angles α and β. The numerical results are available for cases with $\phi \leq 35°$, and geotechnical engineers can use them in the preliminary design stage. Based on upper bound limit analysis using the NS-FEM, some concluding remarks can be shown as follows:

- There are two distinct failure modes for the slope stability analysis, i.e. the base failure mode and the toe failure mode. The base failure was commonly encountered for slight friction angles $\phi \leq 5^{\circ}$ and $\beta \leq 60^{\circ}$, and the failure mechanisms extend beneath the toe of the slope. In contrast, a toe failure generally occurs for a slope with a larger soil friction angle, and the sliding surface passes through the toe of the slope.

- In general, the stability numbers N_s decrease continuously with increasing the slope inclination angle α and β, and it increases with rising friction angle ϕ. The obtained results agree with the average values of the lower and upper bound reported by Lyamin and Sloan [20, 21], Chen [8], Makrodimopoulous & Martin [36]. It demonstrates that the present method is highly effective for solving slope stability analysis in cohesive-frictional soils.

References

[1] Janbu, N. (1973). Slope stability computations. In *Embankment Dam Engineering*, John Wiley and Sons, New York, 47–86.

[2] Morgenstern, N. R., Price, V. E. (1965). The analysis of the stability of general slip surfaces. *Géotechnique*, 15(1):79–93.

[3] Spencer, E. (1967). A method of analysis of the stability of embankments assuming parallel inter-slice forces. *Géotechnique*, 17(1):11–26.

[4] Sarma, S. K. (1973). Stability analysis of embankments and slopes. *Géotechnique*, 23(3):423–433.

[5] Fredlund, D. G., Krahn, J. (1977). Comparison of slope stability methods of analysis. *Canadian Geotechnical Journal*, 14(3):429–439.

[6] Chen, Z.-Y., Morgenstern, N. R. (1983). Extensions to the generalized method of slices for stability analysis. *Canadian Geotechnical Journal*, 20(1):104–119.

[7] Drucker, D. C., Prager, W., Greenberg, H. J. (1952). Extended limit design theorems for continuous media. *Quarterly of Applied Mathematics*, 9(4):381–389.

[8] Chen, W.-F. (2013). *Limit analysis and soil plasticity*. Elsevier.

[9] Michalowski, R. L. (1995). Slope stability analysis: a kinematical approach. *Géotechnique*, 45(2):283–293.

[10] Donald, I. B., Chen, Z. (1997). Slope stability analysis by the upper bound approach: fundamentals and methods. *Canadian Geotechnical Journal*, 34(6):853–862.

[11] Kim, J., Salgado, R., Yu, H. S. (1999). Limit analysis of soil slopes subjected to pore-water pressures. *Journal of Geotechnical and Geoenvironmental Engineering*, 125(1):49–58.

[12] Liu, F., Zhao, J. (2013). Limit analysis of slope stability by rigid finite-element method and linear programming considering rotational failure. *International Journal of Geomechanics*, 13(6):827–839.

[13] bin Sun, Z., bing Qin, C. (2014). Stability analysis for natural slope by kinematical approach. *Journal of Central South University*, 21(4):1546–1553.

[14] Seyed-Kolbadi, S., Sadoghi-Yazdi, J., Hariri-Ardebili, M. (2019). An improved strength reduction-based slope stability analysis. *Geosciences*, 9(1):55.

[15] Vu-Hoang, T., Vo-Minh, T., Nguyen-Xuan, H. (2018). Bubble-enhanced quadrilateral finite element formulation for nonlinear analysis of geotechnical problems. *Underground Space*, 3(3):229–242.

[16] Vo-Minh, T. (2021). A bubble-enhanced quadrilateral finite element for estimation bearing capacity factors of strip footing. *Journal of Science and Technology in Civil Engineering (STCE) - NUCE*, 15(2): 77–89.

[17] Sloan, S. W. (1988). Lower bound limit analysis using finite elements and linear programming. *International Journal for Numerical and Analytical Methods in Geomechanics*, 12(1):61–77.

[18] Sloan, S. W. (1989). Upper bound limit analysis using finite elements and linear programming. *International Journal for Numerical and Analytical Methods in Geomechanics*, 13(3):263–282.

[19] Sloan, S. W., Kleeman, P. W. (1995). Upper bound limit analysis using discontinuous velocity fields. *Computer Methods in Applied Mechanics and Engineering*, 127(1-4):293–314.

[20] Lyamin, A. V., Sloan, S. W. (2002). Lower bound limit analysis using non-linear programming. *International Journal for Numerical Methods in Engineering*, 55(5):573–611.

[21] Lyamin, A. V., Sloan, S. W. (2002). Upper bound limit analysis using linear finite elements and non-linear programming. *International Journal for Numerical and Analytical Methods in Geomechanics*, 26 (2):181–216.

[22] Krabbenhoft, K., Lyamin, A. V., Hjiaj, M., Sloan, S. W. (2005). A new discontinuous upper bound limit analysis formulation. *International Journal for Numerical Methods in Engineering*, 63(7):1069–1088.

[23] Hughes, T. J. R., Cohen, M., Haroun, M. (1978). Reduced and selective integration techniques in the finite element analysis of plates. *Nuclear Engineering and Design*, 46(1):203–222.

[24] Piltner, R., Taylor, R. L. (2000). Triangular finite elements with rotational degrees of freedom and enhanced strain modes. *Computers & Structures*, 75(4):361–368.

[25] Simo, J. C., Rifai, M. S. (1990). A class of mixed assumed strain methods and the method of incompatible modes. *International Journal for Numerical Methods in Engineering*, 29(8):1595–1638.

[26] Cardoso, R. P. R., Yoon, J. W., Mahardika, M., Choudhry, S., de Sousa, R. J. A., Valente, R. A. F. (2007). Enhanced assumed strain (EAS) and assumed natural strain (ANS) methods for one-point quadrature solid-shell elements. *International Journal for Numerical Methods in Engineering*, 75(2):156–187.

[27] Liu, G. R., Nguyen-Thoi, T., Nguyen-Xuan, H., Lam, K. Y. (2009). A node-based smoothed finite element method (NS-FEM) for upper bound solutions to solid mechanics problems. *Computers & Structures*, 87 (1-2):14–26.

[28] Nguyen-Xuan, H., Rabczuk, T., Nguyen-Thoi, T., Tran, T. N., Nguyen-Thanh, N. (2011). Computation of limit and shakedown loads using a node-based smoothed finite element method. *International Journal for Numerical Methods in Engineering*, 90(3):287–310.

[29] Wu, S. C., Liu, G. R., Zhang, H. O., Xu, X., Li, Z. R. (2009). A node-based smoothed point interpolation method (NS-PIM) for three-dimensional heat transfer problems. *International Journal of Thermal Sciences*, 48(7):1367–1376.

[30] Liu, G. R., Chen, L., Nguyen-Thoi, T., Zeng, K. Y., Zhang, G. Y. (2010). A novel singular node-based smoothed finite element method (NS-FEM) for upper bound solutions of fracture problems. *International Journal for Numerical Methods in Engineering*, 83(11):1466–1497.

[31] Wang, G., Cui, X. Y., Feng, H., Li, G. Y. (2015). A stable node-based smoothed finite element method for acoustic problems. *Computer Methods in Applied Mechanics and Engineering*, 297:348–370.

[32] Vo-Minh, T., Nguyen-Minh, T., Chau-Ngoc, A. (2018). Upper bound limit analysis of circular tunnel in cohesive-frictional soils using the node-based smoothed finite element method. In *Proceedings of the International Conference on Advances in Computational Mechanics 2017*, Springer Singapore, 123–141.

[33] Vo-Minh, T., Nguyen-Minh, T., Chau-Ngoc, A., Nguyen-Chanh, H. (2017). Stability of twin circular tunnels in cohesive-frictional soil using the node-based smoothed finite element method (NS-FEM). *Journal of Vibroengineering*, 19(1):520–538.

[34] Vo-Minh, T., Chau-Ngoc, A., Nguyen-Minh, T., Nguyen-Chanh, H. (2018). A node-based smoothed finite element method for stability analysis of dual square tunnels in cohesive-frictional soils. *Scientia Iranica*, 25(3):1105–1121.

[35] Vo-Minh, T. (2019). Calculation of bearing capacity factors of strip footing using the nodebased smoothed finite element method (NS-FEM). In *Lecture Notes in Civil Engineering*, Springer Singapore, 1127–1134.

[36] Makrodimopoulos, A., Martin, C. M. (2007). Upper bound limit analysis using simplex strain elements and second-order cone programming. *International Journal for Numerical and Analytical Methods in Geomechanics*, 31(6):835–865.

[37] Mosek. *The MOSEK optimization toolbox for MATLAB manual*.